Structure determination of the transactivation domain of p53 in complex with S100A4 using annexin A2 as a crystallization chaperone

Péter Ecsédi[1], Gergő Gógl[1,2], Henrietta Hóf[1], Bence Kiss[1], Veronika Harmat[3] and László Nyitray[1] *

[1] Department of Biochemistry, ELTE Eötvös Loránd University, Budapest, Hungary
[2] Institute of Genetics and of Molecular and Cellular Biology, IGBMC, Strasbourg, France
[3] ELTE Eötvös Loránd University, Institute of Chemistry, MTA-ELTE Protein Modeling Research Group, Budapest, Hungary

* To whom correspondence may be addressed. E-mail: nyitray@elte.hu.

Abstract

In spite of the fact that structure solving methods are constantly improving, the biggest challenge of protein crystallography remains the production of well diffracting single protein crystals. Full understanding the environmental factors that influence crystal packing would be an enormous task, therefore crystallographers are still forced to work “blindly” trying as many crystallizing conditions and mutations, designed to improve crystal packing, in the sequence of the target protein as possible. Numerous times the random attempts simply fail even when using crystallization robots or recent techniques to determine the optimal mutations. As an alternative option in these cases, crystallization chaperones can be used. These proteins have a unique property, namely they easily form protein crystals, which can be exploited by using them as a heterologous fusion partner to promote crystal contact formation. Today, the most frequently used crystallization chaperone is the maltose-binding protein (MBP) and crystallographers are in need of other options. Our previous results showed the outstanding crystallization properties of a non-EF hand calcium-binding protein annexin A2 (ANXA2). Here, we compared ANXA2 with the wild type MBP and found that ANXA2 is just as good, if not a better crystallization chaperone. Using ANXA2 for this purpose, we were able to solve the atomic resolution structure of a challenging crystallization target, the transactivation domain (TAD) of p53 in complex with S100A4, an EF hand calcium-binding protein associated with metastatic tumors. The full-length TAD forms an asymmetric fuzzy complex with S100A4 and could interfere with its function.

Introduction

Structural biology methods provide powerful tools to understand protein functions and the underlying mechanisms. Protein crystallography is still the most important technique in this field and as structure solving methods have become more and more advanced, the production of high-quality diffracting crystals remains the largest challenge for crystallographers. The process of crystallization is affected by numerous factors including the chemical characteristics of the protein, environmental factors and conformational heterogeneity [1]. For crystallization, usually high amount of purified protein is also required. A popular method to facilitate protein expression and purification is using affinity tags like His_6-tag [2], maltose binding protein (MBP) [3], glutathione-S transferase (GST) [4], thioredoxin (TRX) [5] or several other short peptides or stable proteins fused to the target proteins [6]. Before crystallization, these affinity tags are usually removed using site-specific proteases, which may lead to the precipitation and/or the activity loss of the target molecule [7]. A possible way to avoid these problems and increase the solubility of the target protein is to fuse it to the affinity tag via a short, rigid spacer (lacking any protease cleavage site). This way the conformational heterogeneity of the fusion construct is reduced, which might promote crystallizability and thus the crystallization ability of the chimeric tag can be exploited [8]. Additionally, the known structure of the chimeric tag might be used during data processing to facilitate molecular replacement and structural refinement. For this purpose, MBP, GST and TRX have been used successfully [9, 10], together with other well-crystallizing proteins such as lysozyme [11-13] or antibody fragments [14, 15]. However, so far only MBP appears to be a generally effective crystallization chaperone and at the same time a useful affinity tag [10, 16], and little effort was made to find alternatives that might be equally or even more adequate for this dual role. The number of structures in the PDB using crystallization chaperones is increasing, indicating that this approach can be a highly efficient tool for crystallographers solving the structures of hardly crystallizable proteins or protein complexes. A good example for such a difficult target, is the complex between p53 transactivation domain (TAD) and S100A4.

S100A4 is a small, dimeric EF-hand Ca^{2+}-binding protein known by its pathological role in several metastatic tumors and inflammatory diseases [17]. Its interaction with p53 transactivation domain (TAD, 1-64) has been studied by several groups previously [18-22], however the structure of the complex remains unknown. Note that several other S100 proteins (S100A1, S100A2, S100A4, S100A6, S100A11 and S100B) also bind to p53 TAD [23] or to the C-terminal end of p53 containing the tetramerization (TET, 326-356) and the negative regulatory domains (NRD, 364-393) [21, 24]. S100A4 is a highly soluble protein, even the name S100 refers to the fact that these proteins remain in solution when saturated ammonium sulfate is used [25]. This ability makes S100 proteins immensely difficult to crystallize in general, but in case of p53 the process is even more formidable. In the PDB only NMR structures were published so far containing the whole p53 TAD, which contains both TAD1 (1-41) and TAD2 (42-64) subdomains [26], in complex with a target protein [27-33]. The absence of X-ray structures including the long TAD, despite the large number of studies, shows that the crystallization of this domain in any protein complex is an inherently difficult task. Remarkably, here using annexin A2 (ANXA2) as a crystallization chaperon we were able to solve the atomic resolution structure of this S100A4 – p53 TAD complex.

ANXA2 is a non-EF-hand Ca^{2+}-binding protein [34]. Its ability to aggregate ("annex") phospholipid membranes in a Ca^{2+}-dependent manner underlies its biological functions such as vesicular transport, exo- and endocytosis [34, 35]. ANXA2 consists of a disordered N-terminal (NTD, 2-33) and a highly conserved, rigid C-terminal "core" domains (CTD, 34-339). The convex side of the CTD is responsible for Ca^{2+}-dependent membrane binding while the concave side directs membrane aggregation, as well as binds and anchors the NTD via a highly conserved G-[TS]-[VI] motif localized in the C-terminus of the NTD (C-NTD, 23-33) [36]. ANXA2 is a highly soluble and stable protein and its ability to easily form crystals has recently been observed in our laboratory [36]. Moreover, beside the case of S100A4 – p53 TAD complex studied here, we have already used

ANXA2 previously to determine the structure of a PDZ domain with a bound peptide ligand [37]. Results presented in this paper suggest that ANXA2 could be another promising crystallization helper molecule similarly to MBP and it is likely applicable to determine the structure of other difficult protein complexes.

Results

In vitro characterization of the p53 TAD – S100A4 complex

The first 60 residues of p53, known as the transactivation domain (TAD^{1-60}) [26] was expressed as a recombinant protein and used in the binding experiments. It was found, using isothermal titration calorimetry (ITC) measurements, that the interaction between p53 TAD^{1-60} and S100A4 is asymmetric (a single peptide binds to one S100A4 dimer) and its dissociation constant is in the micromolar range (Fig. 1. A). According to our circular dichroism (CD) measurements, analyzed with the BesStSel secondary structure prediction program [38], the structure of the originally disordered TAD^{1-60} peptide changes to a more helical structure upon complex formation with S100A4 (α-helix content increases from ~4.6% to ~29.4%) (Fig. 1. B). Similar effect was observed with other S100 ligands [21, 39]. Previously, Lee *et. al.* found several regions in apo p53 TAD peptide with relatively high secondary structure propensity (residues 18-26, 40-44 and 48-53) using NMR spectroscopy [40] (Fig. 1. C). The number of residues in these transiently formed nascent structural elements are in good agreement with the CD data presented here. Disordered binding regions (IDRs) of proteins usually fold upon binding [41], therefore one can assume that those short-term observed folds of TAD could be the key elements in complex formation [42]. Nevertheless, the low overall helix propensity of the peptide even in the bound form predicts that TAD probably retains partial flexibility and forms a dynamic, partially folded so-called "fuzzy" complex [43] with S100A4. These results together with other findings [22, 23] suggest that the first 16 and the last 3 residues do not participate in the interaction. Therefore, a truncated TAD peptide (residues 17-56, TAD^{17-56}) was produced and its binding to S100A4 was evaluated using competitive fluorescence polarization (FP) assay. It revealed that the truncated TAD^{17-56} has the same affinity to S100A4 as the longer TAD^{1-60} peptide (K_d values: ~0.7 and 0.9 μM respectively) (Fig. 1. D). Thus the subsequent experiments were conducted using this "minimal" binding sequence of p53.

Designing the C-terminal ANXA2 fusion constructs

We have made several attempts to crystallize p53 TAD^{17-56} – S100A4 complex alone or by using GST or wild type MBP (wtMBP) tags as crystallization chaperones (connected by an "SGSGG" short linker). If either p53 TAD^{17-56} or S100A4 was fused to GST or MBP, respectively, then mixed with the other partner, no crystal was observed in any case. The poor crystal forming ability of the complex presumably comes from the high solubility of S100A4 and the dynamic, fuzzy binding mode of p53. Following these unavailing attempts, two fusion constructs of ANXA2 were designed, based on its 3D structures [36, 37], and cloned into a modified pET15 vector together with an N-terminal short multi-cloning site (for inserting the target proteins) followed by a cleavable His_6-tag with the aim of using it as a crystallization chaperone similarly to MBP/GST. One construct ($ANXA2^{23-339}$) contains the so-called C-NTD of ANXA2 that transiently binds to the core domain (Fig. 2. A). Its presence considerably stabilizes ANXA2 [36], thus facilitates crystal formation, however, its structural plasticity may results in a less compact fold with a long disordered linker between the target protein and ANXA2. The other construct ($ANXA2^{29-339}$) does not contain the C-NTD (Fig. 2. B), which precludes the formation of such a long spacer but results a less stable core domain (DNA sequences and ANXA2 containing plasmids were uploaded and sent to Addgene with IDs of 136543, 136544, 136545 and 136546).

In a previously published paper, where we solved the crystal structure of the second PDZ domain of the membrane-associated guanylate kinase (Magi-1), the former ANXA2 construct was used [37]. In case of p53 TAD$^{17-56}$ we had to apply the latter strategy since S100A4 interacts with the C-NTD of ANXA2 [36]. To increase the chance of crystal formation, we have produced a chimera where a single-chain S100A4Δ8 dimer (scS100A4Δ8) was fused to ANXA2$^{29-339}$, using the previously designed vectors. In case of scS100A4Δ8 the last 8 residues forming a short disordered region, thus presumably negatively affecting crystal formation, were deleted and the two subunits were covalently joint into a single-chain construct (a short linker with the sequence of "SAGSAG" was used between the subunits). Using this chimera, ANXA2 could drive crystal packing instead of the highly soluble S100A4. In our first attempts, where this scS100A4Δ8 – ANXA2$^{29-339}$ construct was complexed with p53 TAD$^{17-56}$, the p53 peptide ligand dissociated from the crystals and only the scS100A4Δ8 – ANXA2$^{29-339}$ chimera was found in apo form (not deposited in the PDB). We believe that the presence of the fuzzy interaction is unfavorable for crystal formation, thus crystals lacking p53, caused by the temporary dissociation of the peptide, could form more easily causing the elimination of the peptide from its binding site in those structures. To solve this problem we covalently bound p53 TAD$^{17-56}$ to the N-terminus of scS100A4Δ8 – ANXA2$^{29-339}$ via a GS linker ("GGSG" plus "HM" as cloning artifact) (Fig. 2. C) to form the ternary chimeric construct of p53 TAD$^{17-56}$ – scS100A4Δ8 – ANXA2$^{29-339}$. Note here that the artificially produced scS100A4Δ8 allowed the presence of only one covalently bound ANXA2$^{29-339}$ and p53 TAD$^{17-56}$ in the chimera.

Solving the crystal structure of p53 TAD – S100A4 complex

Using the p53 TAD$^{17-56}$ – scS100A4Δ8 – ANXA2$^{29-339}$ construct we could solve the structure of the complex at 3.1 Å resolution (Fig. 3. A) (Table 1.). Two chimeric molecules were found in the asymmetric unit. In both chains, ANXA2$^{29-339}$ was visible, but in chain B the scS100A4Δ8 was presumably very flexible and the electron density map of the complex was very weak. In case of chain A, however, both scS100A4Δ8 and the p53 fragment could be built into the electron density map. The electron density of the linkers between p53 TAD$^{17-56}$ and scS100A4Δ8, as well as between the S100A4 subunits were not visible indicating that those additional residues did not affect the binding mode of p53 TAD$^{17-56}$ to scS100A4Δ8. Three short segments of p53 were observed in the structure to be in α-helical conformation. The residues of these observed helices nicely overlap with the residues of the nascent secondary elements and forming helices previously found by others in apo [40] or in complexed p53 [33]. The N-terminal α-helix (18-25), part of TAD1, makes exclusively hydrophobic interactions (F19, L22, W23, and L25 of p53) with one of the binding pocket of S100A4 dimer. Note that S20/D21 and K24 of p53 form an intramolecular salt bridge stabilizing this α-helix. At the C-terminal end of the TAD segment, two more α-helices (residues 37-42 and 47-53) are visible in the complex. S37 and S46 N-terminally cap the evolved helices respectively, further stabilizing their structure. Hydrophobic sidechains of L43, L45, I50, W53 and F54 of TAD2 appear to be key residues in anchoring this region to S100A4. The large aromatic side chain of W53 nicely fits into the hydrophobic environment, formed by F45/F89 of the corresponding subunit and I50/F54 of TAD2, while L43 and L45 of TAD2 face to the binding pocket of S100A4. Results of our alanine scanning experiments (Fig. 3. B and C) confirmed the importance of this region. Mutation of I50, W53 or F54 to alanine caused significant decrease in affinity (K_d values increased ~11, ~62 and ~29 times, respectively, compared to the wild type peptide). Mutation of 22L, 23W and L43 caused similar effects (K_d values increased ~11, ~16 and ~16 times, respectively). Matching decrease in affinity was observed by van Dieck *et. al*. using L22/Q and W23/S mutants [23]. These data show that p53 TAD anchors to S100A4 mostly by the above residues while other hydrophobic amino acids, namely F19, L25, L26 and L45 further strengthen the interaction (their Ala substitution increases the K_d 4-10 times). Interestingly, the deletion of the middle segment (p53 DEL: residues 31-35, -VLSPL-), which could not be built into the electron density map, hence it might not take part in the interaction with S100A4 despite it contains several hydrophobic residues, decreased the affinity by one order of

magnitude. This observation suggests that the middle region of the peptide ligand binds to S100A4 transiently resulting the fuzziness of the complex.

Comparing the crystal forming ability of ANXA2 and wtMBP

To assess the usability of ANXA2 as a crystallization chaperone, we first compared the crystal forming abilities of wtMBP and ANXA2. For this purpose 8 constructs were produced: scS100A4Δ8 and the second PDZ domain of Magi-1 (PDZ) (previously crystallized, fused to ANXA2 [37]) as target proteins; the crystallization chaperones, wtMBP and $ANXA2^{29-339}$ alone; and the combinations of the target and chaperone proteins (wtMBP-PDZ, wtMBP-scS100A4Δ8, PDZ-$ANXA2^{23-339}$ and scS100A4Δ8-$ANXA2^{29-339}$). 8 (SSSNNNTS) and 25 residues long (SSSNNNTSGCGGGGGSMSENLYFQG) linker sequences were applied in case of wtMBP-scS100A4Δ8 and wtMBP-PDZ constructs, respectively. The linkers between wtMBP and target proteins were 4 residues long in case of the largest group of reported structures [9, 10], though certainly it is also a subject of optimization in our cases, however several structures were reported using longer linkers [10]. The PDZ domain represents a smaller (~100 residues) while scS100A4Δ8 a larger (~200 residues) target protein. Using Morpheus and JCSG+ screens we determined the number of conditions in which each construct gave observable crystals (Fig. 4.). Based on the results of previous ANXA2 crystallizations, all constructs were used at 250 μM (~8-15 mg/ml for $ANXA2^{29-339}$ and ANXA2 constructs) concentration before mixing, but in case of wtMBP and wtMBP chimeras the concentration was increased to 2 mM (~82-120 mg/ml) since no crystals were observed during the first screening when lower amount (~10-15 mg/ml) was used. Free target proteins could not form crystals at all. WtMBP formed crystals in 14 out of 192 conditions (~7 %) while this ratio was ~44 % in the case of $ANXA2^{29-339}$ (84/192). This extremely good crystal forming ability was also observed in case of PDZ-$ANXA2^{23-339}$ (49/192) (~25 %), however scS100A4Δ8-$ANXA2^{29-339}$ crystallized relatively poorly (9/192) (~4 %). The wtMBP chimeras formed no crystals even at the elevated concentration. The crystal formation was monitored for a month in all samples, however no change was observed after a week. To measure the critical concentration of each constructs for crystallogenesis, dilution series of the proteins (using the sample buffer for dilution) were mixed with some of those conditions where crystals were found in the previous experiment (Fig. 5.). While wtMBP formed crystals only above 500 μM (~20.5 mg/ml) concentration, $ANXA2^{29-339}$ and PDZ-$ANXA2^{23-339}$ could be crystallized at as low concentration as 7 μM (~0.25 and 0.34 mg/ml respectively). The scS100A4Δ8-$ANXA2^{29-339}$ chimera behaved differently as no crystal growth was observed under 125 μM (~7.5 mg/ml). Note here that other groups previously crystallized MBP at as low concentration as 3.5 mg/ml [44]. It is also noteworthy however, that we used no mutations in the crystallization chaperone to help crystal formation and in our study only simple screening conditions were tested without any additive or optimization. These might also have improved our MBP results. Overall though, these experiments provide a proof-of-concept that ANXA2 is a very good candidate to use as a crystallization chaperon.

Discussion

Currently one of the most challenging step of protein crystallography is the production of protein crystals. Firstly, the number of deposited structures in the PDB increases, therefore, and naturally, the amount of unsolved but easily crystallizable molecules and complexes decreases. Secondly, the toolbox of crystal solving methods are continuously developing, while the formation of crystals is still unpredictable and crystallization is attempted by brute force, screening tremendous amount of conditions [45] or by designing scores of mutations [46, 47]. As an alternative, recombinant crystallization chaperones like MBP, which is most commonly used for this purpose [10], can be fused to the target protein or complexed to facilitate the growth of crystals. Apparently, the repertoire of usable crystallization helper proteins is very small. MBP has several unquestionable advantages. It is highly soluble, therefore enhances the solubility of the target molecules raising the yield of

protein expression. However, for the same reason it also increases the concentration dependence of crystal formation. It can be applied as a specific purification tag and it clearly has an above-average crystal forming ability. However, alone this MBP fusion system cannot fulfill the needs of crystallographers as this system has its own limitations [48]. Thus, exploring novel or even better crystallization chaperones might help to by-pass the bottleneck of crystallography: the production of well diffracting crystals. We show here that ANXA2, a Ca^{2+} and membrane binding protein might be the next candidate for this purpose.

Compared to wtMBP, ANXA2 is also a highly soluble protein with a compact and stable structure. Our data shows that ANXA2 has a significantly better crystallizing ability compared to wtMBP. It forms crystals at very low concentrations and it is widely permissive to crystallization conditions. ANXA2 can also be used as a purification tag owing to its calcium dependent heparin binding activity, a property shared only by a few other proteins such as serum amyloid P component, P- and L-selectins and ANXA5 [49, 50]. Utilizing this ability of ANXA2, a heparin column can be used for a specific affinity-based purification [50, 51]. ANXA2 and thus likely ANXA2-based chimeras can also be specifically purified using only anion and cation exchange columns and omitting affinity chromatography as previously described [36].

Crystal packing and the limitation of the ANXA2 chaperone system

To understand the remarkable crystal forming ability of ANXA2, several ANXA2 structures in the PDB were analyzed (Fig 6. and 7.). It appears that ANXA2 forms one type of crystal packing interaction in most cases. In the crystals ANXA2 molecules build a spiral like structure with a Ca^{2+} partially coordinated by the carbonyl groups of M278, G280, G282 and the carboxyl group of D322 from one molecule (molecule A) (Fig. 7.) and partially by the carboxyl group of S234 of another ANXA2 (molecule B). Note that ANXA2 could form crystals differently depending on its partner (Fig. 6. E). Interestingly, this type of co-coordination of Ca^{2+} in the crystal exists mostly in case of ANXA2 structures in the family. ANXA1 [52] (PDB:1MCX) and bovine ANXA6 [53] (PDB:1AVC) are exceptions where D196 and 237D of molecule B completes the number of coordinating residues of molecule A. Other contacts further strengthen this intermolecular interaction. Residues of E189 (B), D192 (B), R196 (B), K312 (A), Y317 (A) and Q321 (A) form a chain of salt bridges, while Y188 (B) and Y311 (A) make stacking interactions (Fig. 7.). Importantly, the crystal packing of ANXA2 is not tight and large solution channels appear between molecules. Analyzing the structures of PDZ-$ANXA2^{23-339}$ [37] and p53 TAD^{17-56}–scS100A4Δ8–$ANXA2^{29-339}$ chimeras, the difference is clearly visible. The PDZ domain (~100 residues) can easily fit into these channels but the scS100A4Δ8 (~200 residues) is too large and must find an alternative position (Fig 6.), which hampers crystal formation but still does not inhibit it entirely as was observed in the screening experiments. This comparison of PDZ and scS100A4Δ8 chimeras shows some limitation of this system, namely the size of the target protein.

If the target molecules are too large or the crystals diffract poorly, other strategies are worth considering. In case of protein–peptide complexes, instead of the target protein, the target peptide can be fused to ANXA2 and the peptide–ANXA2 construct should be complexed with the partner protein. Another possible strategy is to fuse the target protein to ANXA2 without any flexible linker in a way where the last helix of the target is continuous with the first helix of ANXA2. Similar modification was suggested and used by Tengchuan *et. al.* producing a MBP–IPS-1 CARD construct [9]. It decreased the mobility of the target protein and improved the quality of their diffraction data. Moreover, similarly to MBP [54], some specific modifications in the sequence of ANXA2 might further increase its crystal forming ability or the sizes of solution channels. One possible way could be to exchange S234 (B molecule) to D/E234 and in parallel mutate D322 (A molecule) to serine to increase the Ca^{2+} co-coordinating effect of molecule B.

Structure of the fuzzy p53 TAD – S100A4 complex determined with ANXA2 as crystallization chaperone

In this work, we have solved the structure of a highly challenging crystallization target, the p53 TAD – S100A4 complex using ANXA2 as crystallization chaperone. As mentioned above, no X-ray structure containing both TAD1 and TAD2 subdomains of p53 is available in the PDB. The new structure reveals that the intrinsically disordered TAD forms three short α-helices upon interacting with S100A4. Interestingly, these α-helices are remarkably similar to other TAD complexes determined by NMR spectroscopy, such as p53 – p300 [29], p73 – MDM2 [55], p53 – HMG-box [28] and p53 – CBP [33]. This highlights the versatility of p53 TAD and explains the observed transient fuzzy binding mode, since it must form interactions with a large number of partners. It would be interesting to solve the above structures using X-ray with a full-length TAD peptide. Based on our results, ANXA2 could be an ideal chaperone for successful crystallization of these other fuzzy complexes.

The function of the p53 TAD – S100A4 complex in cell is not yet clear [18, 20]. TAD has moderate affinity towards S100A4 and it interacts with several other regulatory proteins with similar or higher affinities [56-58]. These observations suggest that TAD is presumably bound to other partner proteins than S100A4. Nevertheless, in various metastatic tumors S100A4 concentrations were found to be elevated by several order of magnitudes [59, 60]. This increase in expression levels and several posttranslational modifications on p53 [23] might be sufficient for disturbing the normal function of p53 system by blocking the interactions of TAD with other regulatory proteins.

Materials and methods

Cloning, protein expression and purification

N-terminally truncated forms of human ANXA2 (23-339 and 29-339) (UniProt code: P07355), along with a short multi-cloning site, were cloned into a modified pET15 vector (pEV) that contains an N-terminal tobacco etch virus (TEV)-cleavable His_6-tag (pANXA2$^{23-339}$ and pANXA2$^{29-339}$). Human p53 TAD$^{1-60}$ and p53 TAD$^{17-56}$ (UniProt code: P04637) was cloned into a modified pGEX vector (pETARA) containing an N-terminal TEV-cleavable glutathione *S*-transferases (GST). QuikChange method was used to produce the p53 TAD$^{17-56}$ and the cys-p53 TAD$^{17-56}$ peptide mutants. The second PDZ domain of human Magi-1 protein (PDZ) (Uniprot code: Q96QZ7) was cloned previously by Gógl *et. al. [37]*. Single-chain human S100A4Δ8 (UniProt code: 26447) insert (consisting the two S100A4Δ8 subunit connected by a 6-residue-long GS-linker) was cloned into the pANXA2$^{29-339}$, pET-MBP and pEV vectors. In case of p53 TAD$^{17-56}$ – scS100A4Δ8 – ANXA2$^{29-339}$ construct, the p53 TAD$^{17-56}$ was cloned N-terminally to the scS100A4Δ8 in the scS100A4Δ8-pANXA2$^{29-339}$ construct with a 6-residue-long GS linker. The wild type S100A4, wtMBP-PDZ and ANXA2 proteins were previously cloned as described in: [36, 37, 39].

WtMBP, wtMBP – PDZ, wtMBP – scS100A4Δ8, ANXA2$^{29-339}$, PDZ – ANXA2$^{23-339}$, scS100A4Δ8 – ANXA2$^{29-339}$, p53 TAD$^{17-56}$ – scS100A4Δ8 – ANXA2$^{29-339}$, scS100A4Δ8, PDZ and p53 TAD constructs were expressed in *E. coli* BL21(DE) cells. Transformed cultures were grown in Luria-Bertani (LB) broth supplemented with 100 μg/ml ampicillin at 37 °C until the optical density at 600 nm reached 0.8. Expression was induced with 0.25 mM isopropyl β-D-1-thiogalactopyranoside (IPTG) at 18°C overnight or at 28°C for 4 hours in case of GST-fusions. Pelleted cells were disintegrated by ultrasonication in a buffer containing 20 mM Tris, pH 8, 300 mM NaCl, 0.1 mM tris(2-carboxyethyl)phosphine (TCEP), and 1 mM phenylmethanesulfonyl fluoride (PMSF). Cell lysates were clarified by centrifugation at 48,000 × *g*, and the supernatant was applied to Ni^{2+}-affinity chromatography column using Profinity IMAC resin (Bio-Rad) with 20 mM Tris, pH 8, 300 mM

NaCl, 0.1 mM TCEP as wash buffer. His_6-tagged proteins were eluted with the wash buffer complemented with 250 mM imidazole. GST-fusions expressing cells were resuspended in a buffer containg 150 mM NaCl. After ultrasonication, the clarified cell lysates were loaded onto Protino Glutathione Agarose 4B resin (Macherey-Nagel). After thorough wash with the lysis buffer the GST-fusions were eluted using the washing buffer complemented with 10 mM reduced glutathione. GST and His_6-tag were eliminated using TEV protease at room temperature overnight. Note that the His_6-tag was not removed from MBP-fusions. After complete cleavage, GST was removed from solution by heat denaturation followed by centrifugation. p53 fragments were further purified by reverse HPLC using a Jupiter 300 C5 column (Phenomenex). The p53 conataining fractions were lyophilized and stored at -20 °C. MBP, MBP – PDZ and MBP – scS100A4Δ8 constructs were further purified using MBP affinity purification (Amylose Resin, NEB) and eluted using 10 mM maltose in the washing buffer, than concentrated by Milicon ultra filter and stored at -80 °C. Following the removal of His_6-tag using reverse Ni^{2+}-affinity chromatography $ANXA2^{29-339}$, PDZ – $ANXA2^{23-339}$, scS100A4Δ8 – $ANXA2^{29-339}$ and p53 TAD^{17-56} – scS100A4Δ8 – $ANXA2^{29-339}$ were dialyzed and separated by cation-exchange chromatography using HiTrap SP HP column at pH 6.5. ScS100A4Δ8 were applied to phenyl-Sepharose 6 resin column (GE Healthcare), washed with 20 mM HEPES, 50 mM NaCl, 0.5 mM $CaCl_2$, 0.1 mM TCEP, and eluted with the wash buffer supplemented with 5 mM EGTA. The recombinant proteins were concentrated using Amicon Ultra-15 Centrifugal Filter Units and stored at -80 °C.

Fluorescent labeling

Cys-p53 TAD^{17-56} peptide was labeled selectively at the artificially cloned N-terminal Cys residue with a 3-fold excess of 5-(iodoacetamido)-fluorescein (5-IAF, Sigma-Aldrich) in 20 mM Hepes pH 7.5, 150 mM NaCl, 1 mM TCEP buffer incubating the samples for 18 hours in the dark at 4 °C. The fluorescein-conjugated p53 TAD^{17-56} (referred as Fl-p53 TAD) was separated from the non-reacted dye and unconjugated peptide by gel filtration (HiTrap Desalting columns, GE) and RP-HPLC using Jupiter 300 C5 column (Phenomenex).

Crystallization, data collection and structure determination

Crystallization samples contained 350 μM p53 TAD^{17-56} – scS100A4Δ8 – $ANXA2^{29-339}$, 20 mM HEPES pH 7.5, 100 mM NaCl, 1mM TCEP and 5 mM $CaCl_2$ before mixing. Crystallization was carried out in standard hanging drop vapor-diffusion set-up at 20 °C, mixing the protein and the precipitant solution in different volumes using distinct protein : precipitant ratios. 1.25 M NaCl was used [61] as reservoir solution. Best crystals grew in the D6 condition of Morpheus screen (Molecular dimension). Crystals were supplemented with 20% glycerol before flash cooling in liquid nitrogen. Data were collected on the PXIII beamline of the Swiss Light Source (Villigen) at 100 K with a wavelength of 1 Å (Table 1.). Data were processed with XDS [62]. The phase problem was solved by molecular replacement (MR) in PHASER [63] with a high resolution structure of S100A4 [64] and ANXA2 [36] as search models. Structure refinement was carried out in PHENIX [65] and structure remodelling/building was done in Coot [66]. Crystal structure was deposited to the Protein Data Bank under the accession code of 6T58.

Crystal screening of chimera constructs

WtMBP, wtMBP – PDZ and wtMBP – scS100A4Δ8 constructs were used in 2 mM (at first in 250 μM), while $ANXA2^{29-339}$, PDZ – $ANXA2^{23-339}$, scS100A4Δ8 – $ANXA2^{29-339}$, scS100A4Δ8 and PDZ were used in 250 μM concentration in 20 mM HEPES pH 7.5, 100 mM NaCl, 1mM TCEP and 5 mM $CaCl_2$ containing buffer before mixing. Samples were dialyzed together before experiments. Note that, Ca^{2+} containing protein solutions may form salt crystals, thus false positive results with some conditions of crystallization screens (especially with phosphates and sulphates). By using Ca^{2+} containing buffers for all protein solutions, the chance for such false hits supposed to be similar for them, so the results can be compared. Crystallization was done in standard hanging drop vapor-diffusion

set-up at 20 °C, mixing the protein and the precipitant solutions of JCSG+ and Morpheus screens (Molecular Dimensions) in equal protein/precipitant volume. In case of screening experiments the reservoir solutions were identical to the precipitant while 1.25 M NaCl was used [61] when the concentration dependence of crystallogenesis was studied. Crystal formation was monitored for a week in the former and for a month in the latter case.

Isothermal titration calorimetry (ITC)

60 μM wild type S100A4 dimer was titrated with p53 TAD^{1-60} peptide (500 μM) at 37 °C in 20 mM HEPES pH 7.5, 150 mM NaCl, 1 mM $CaCl_2$, and 1 mM TCEP containing buffer using a MicroCal VP-ITC instrument. The injection volume was 5 - 5 μL with 400 s time intervals between injections. The Origin for ITC 5.0 (OriginLab) software package was used for data processing, and the model "One Set of Sites" was fitted.

Circular dichroism (CD) spectrometry

Far UV CD spectra of 50 μM p53 TAD^{1-60} and 80 μM wild type S100A4 dimer alone and together were measured in 20 mM HEPES pH 7.5, 20 mM NaCl, 1 mM $CaCl_2$, and 1 mM TCEP containing buffer at 25 °C using a 0.01 cm quartz cuvette (Hellma) in a Jasco J-715 spectropolarimeter. We assumed that the secondary structure of S100A4 does not change upon p53 binding [39], thus the spectra of the bound p53 fragment was produced as the difference between the spectrum of S100A4 - p53 TAD^{1-60} complex and of S100A4 alone. CD spectra of apo and S100A4 bound p53 TAD^{1-60} were analyzed using BeStSel method [38].

Fluorescence polarization (FP) measurements

Measurements were carried out using 20 mM HEPES pH7.5, 150 mM NaCl, 1 mM $CaCl_2$, 0.1 mM TCEP and 0.05% Tween-20 containing buffer. Fluorescence polarization was measured in 384-well plates (Corning #3676) using Synergy H4 multi-mode microplate reader (BioTek). Firstly, the binding affinity of S100A4 to Fl-p53 TAD^{17-56} (50 nM) was determined in a direct binding assay. The quadratic binding equation was used for fitting to data. Based on the result of the direct FP measurement 50 nM Fl-p53 TAD^{17-56} complexed with 2.5 μM wild type S100A4 dimer was titrated with unlabeled wild type $p53^{1-60}$, $p53^{17-56}$ and mutated $p53^{17-56}$ peptides (competitive FP measurements). The competitive binding equation [67] was used for fitting to data. Origin 8 was used for data evaluation. Measurements were carried out in triplicates.

Acknowledgement: We thank the staff members at the beamlines PXIII of SLS for assistance in data collection.

Funding: This work was supported by the National Research Development and Innovation Fund of Hungary (K 119359 to L.N.) Project no. 2018-1.2.1-NKP-2018-00005 has been implemented with the support provided from the National Research Development and Innovation Fund of Hungary, financed under the 2018-1.2.1-NKP funding scheme. This work was completed in the ELTE Institutional Excellence Program supported by the National Research, Development and Innovation Office (NKFIH-1157-8/2019-DT) G.G. was supported by the Post-doctorants en France program of the Fondation ARC.

Author contributions: P.E., G.G., H.H. and B.K. designed and performed research. P.E., G.G., and B.K. analyzed data. P.E., G.G., V.H. and L.N. wrote the paper, L.N. oversaw the research.

Competing interests: The authors declare no conflict of interest.

Data and materials availability: The atomic coordinates have been deposited in the Protein Data Bank, www.pdb.org (PDB IDs: 6T58)

References

1. Tereshko, V., et al., *Toward chaperone-assisted crystallography: protein engineering enhancement of crystal packing and X-ray phasing capabilities of a camelid single-domain antibody (VHH) scaffold.* Protein Sci, 2008. **17**(7): p. 1175-87.
2. Bornhorst, J.A. and J.J. Falke, *Purification of proteins using polyhistidine affinity tags.* Methods Enzymol, 2000. **326**: p. 245-54.
3. Braun, P., et al., *Proteome-scale purification of human proteins from bacteria.* Proc Natl Acad Sci U S A, 2002. **99**(5): p. 2654-9.
4. Smith, D.B., *Generating fusions to glutathione S-transferase for protein studies.* Methods Enzymol, 2000. **326**: p. 254-70.
5. LaVallie, E.R., et al., *Thioredoxin as a fusion partner for production of soluble recombinant proteins in Escherichia coli.* Methods Enzymol, 2000. **326**: p. 322-40.
6. Stevens, R.C., *Design of high-throughput methods of protein production for structural biology.* Structure, 2000. **8**(9): p. R177-85.
7. Baneyx, F., *Recombinant protein expression in Escherichia coli.* Curr Opin Biotechnol, 1999. **10**(5): p. 411-21.
8. Smyth, D.R., et al., *Crystal structures of fusion proteins with large-affinity tags.* Protein Sci, 2003. **12**(7): p. 1313-22.
9. Jin, T., et al., *Design of an expression system to enhance MBP-mediated crystallization.* Sci Rep, 2017. **7**: p. 40991.
10. Waugh, D.S., *Crystal structures of MBP fusion proteins.* Protein Sci, 2016. **25**(3): p. 559-71.
11. Thorsen, T.S., et al., *Modified T4 Lysozyme Fusion Proteins Facilitate G Protein-Coupled Receptor Crystallogenesis.* Structure, 2014. **22**(11): p. 1657-64.
12. Rosenbaum, D.M., et al., *GPCR engineering yields high-resolution structural insights into beta2-adrenergic receptor function.* Science, 2007. **318**(5854): p. 1266-73.
13. Kobilka, B., *The structural basis of G-protein-coupled receptor signaling (Nobel Lecture).* Angew Chem Int Ed Engl, 2013. **52**(25): p. 6380-8.
14. Tamura, R., et al., *Application of the NZ-1 Fab as a crystallization chaperone for PA tag-inserted target proteins.* Protein Sci, 2019. **28**(4): p. 823-836.
15. Lieberman, R.L., et al., *Crystallization chaperone strategies for membrane proteins.* Methods, 2011. **55**(4): p. 293-302.
16. Clifton, M.C., et al., *A Maltose-Binding Protein Fusion Construct Yields a Robust Crystallography Platform for MCL1.* PLoS One, 2015. **10**(4): p. e0125010.
17. Boye, K. and G.M. Maelandsmo, *S100A4 and metastasis: a small actor playing many roles.* Am J Pathol, 2010. **176**(2): p. 528-35.
18. Orre, L.M., et al., *S100A4 interacts with p53 in the nucleus and promotes p53 degradation.* Oncogene, 2013. **32**(49): p. 5531-40.
19. Shen, W., et al., *S100A4 interacts with mutant p53 and affects gastric cancer MKN1 cell autophagy and differentiation.* Int J Oncol, 2015. **47**(6): p. 2123-30.
20. Grigorian, M., et al., *Tumor suppressor p53 protein is a new target for the metastasis-associated Mts1/S100A4 protein: functional consequences of their interaction.* J Biol Chem, 2001. **276**(25): p. 22699-708.
21. Fernandez-Fernandez, M.R., T.J. Rutherford, and A.R. Fersht, *Members of the S100 family bind p53 in two distinct ways.* Protein Sci, 2008. **17**(10): p. 1663-70.
22. van Dieck, J., et al., *Molecular basis of S100 proteins interacting with the p53 homologs p63 and p73.* Oncogene, 2010. **29**(14): p. 2024-35.
23. van Dieck, J., et al., *Posttranslational modifications affect the interaction of S100 proteins with tumor suppressor p53.* J Mol Biol, 2009. **394**(5): p. 922-30.
24. Fernandez-Fernandez, M.R., D.B. Veprintsev, and A.R. Fersht, *Proteins of the S100 family regulate the oligomerization of p53 tumor suppressor.* Proc Natl Acad Sci U S A, 2005. **102**(13): p. 4735-40.
25. Moore, B.W., *A soluble protein characteristic of the nervous system.* Biochem Biophys Res Commun, 1965. **19**(6): p. 739-44.
26. Harms, K.L. and X. Chen, *The functional domains in p53 family proteins exhibit both common and distinct properties.* Cell Death Differ, 2006. **13**(6): p. 890-7.
27. Yoon, M.K., et al., *Cytoplasmic pro-apoptotic function of the tumor suppressor p73 is mediated through a modified mode of recognition of the anti-apoptotic regulator Bcl-XL.* J Biol Chem, 2018. **293**(51): p. 19546-19558.
28. Rowell, J.P., et al., *HMGB1-facilitated p53 DNA binding occurs via HMG-Box/p53 transactivation domain interaction, regulated by the acidic tail.* Structure, 2012. **20**(12): p. 2014-24.
29. Feng, H., et al., *Structural basis for p300 Taz2-p53 TAD1 binding and modulation by phosphorylation.* Structure, 2009. **17**(2): p. 202-10.
30. Okuda, M. and Y. Nishimura, *Extended string binding mode of the phosphorylated transactivation domain of tumor suppressor p53.* J Am Chem Soc, 2014. **136**(40): p. 14143-52.
31. Krauskopf, K., et al., *Regulation of the Activity in the p53 Family Depends on the Organization of the Transactivation Domain.* Structure, 2018. **26**(8): p. 1091-1100 e4.
32. Krois, A.S., et al., *Recognition of the disordered p53 transactivation domain by the transcriptional adapter zinc finger domains of CREB-binding protein.* Proc Natl Acad Sci U S A, 2016. **113**(13): p. E1853-62.
33. Lee, C.W., et al., *Structure of the p53 transactivation domain in complex with the nuclear receptor coactivator binding domain of CREB binding protein.* Biochemistry, 2010. **49**(46): p. 9964-71.
34. Gerke, V. and S.E. Moss, *Annexins: from structure to function.* Physiol Rev, 2002. **82**(2): p. 331-71.
35. Drust, D.S. and C.E. Creutz, *Aggregation of chromaffin granules by calpactin at micromolar levels of calcium.* Nature, 1988. **331**(6151): p. 88-91.
36. Ecsedi, P., et al., *Regulation of the Equilibrium between Closed and Open Conformations of Annexin A2 by N-Terminal Phosphorylation and S100A4-Binding.* Structure, 2017. **25**(8): p. 1195-1207 e5.
37. Gogl, G., et al., *Dynamic control of RSK complexes by phosphoswitch-based regulation.* FEBS J, 2018. **285**(1): p. 46-71.
38. Micsonai, A., et al., *Accurate secondary structure prediction and fold recognition for circular dichroism spectroscopy.* Proc Natl Acad Sci U S A, 2015. **112**(24): p. E3095-103.
39. Kiss, B., et al., *Crystal structure of the S100A4-nonmuscle myosin IIA tail fragment complex reveals an asymmetric target binding mechanism.* Proc Natl Acad Sci U S A, 2012. **109**(16): p. 6048-53.
40. Lee, H., et al., *Local structural elements in the mostly unstructured transcriptional activation domain of human p53.* J Biol Chem, 2000. **275**(38): p. 29426-32.
41. Dunker, A.K., et al., *Intrinsically disordered protein.* J Mol Graph Model, 2001. **19**(1): p. 26-59.
42. Kim, D.H. and K.H. Han, *Transient Secondary Structures as General Target-Binding Motifs in Intrinsically Disordered Proteins.* Int J Mol Sci, 2018. **19**(11).
43. Tompa, P. and M. Fuxreiter, *Fuzzy complexes: polymorphism and structural disorder in protein-protein interactions.* Trends Biochem Sci, 2008. **33**(1): p. 2-8.

44. Duan, X., et al., *Crystal structures of the maltodextrin/maltose-binding protein complexed with reduced oligosaccharides: flexibility of tertiary structure and ligand binding.* J Mol Biol, 2001. **306**(5): p. 1115-26.
45. McPherson, A. and B. Cudney, *Optimization of crystallization conditions for biological macromolecules.* Acta Crystallogr F Struct Biol Commun, 2014. **70**(Pt 11): p. 1445-67.
46. Cooper, D.R., et al., *Protein crystallization by surface entropy reduction: optimization of the SER strategy.* Acta Crystallogr D Biol Crystallogr, 2007. **63**(Pt 5): p. 636-45.
47. Gogl, G., I. Toro, and A. Remenyi, *Protein-peptide complex crystallization: a case study on the ERK2 mitogen-activated protein kinase.* Acta Crystallogr D Biol Crystallogr, 2013. **69**(Pt 3): p. 486-9.
48. Holcomb, J., et al., *Protein crystallization: Eluding the bottleneck of X-ray crystallography.* AIMS Biophys, 2017. **4**(4): p. 557-575.
49. Capila, I. and R.J. Linhardt, *Heparin-protein interactions.* Angew Chem Int Ed Engl, 2002. **41**(3): p. 391-412.
50. Shao, C., et al., *Crystallographic analysis of calcium-dependent heparin binding to annexin A2.* J Biol Chem, 2006. **281**(42): p. 31689-95.
51. Gokhale, N.A., et al., *Phosphoinositide specificity of and mechanism of lipid domain formation by annexin A2-p11 heterotetramer.* J Biol Chem, 2005. **280**(52): p. 42831-40.
52. Rosengarth, A. and H. Luecke, *A calcium-driven conformational switch of the N-terminal and core domains of annexin A1.* J Mol Biol, 2003. **326**(5): p. 1317-25.
53. Avila-Sakar, A.J., C.E. Creutz, and R.H. Kretsinger, *Crystal structure of bovine annexin VI in a calcium-bound state.* Biochim Biophys Acta, 1998. **1387**(1-2): p. 103-16.
54. Moon, A.F., et al., *A synergistic approach to protein crystallization: combination of a fixed-arm carrier with surface entropy reduction.* Protein Sci, 2010. **19**(5): p. 901-13.
55. Shin, J.S., et al., *Structural convergence of unstructured p53 family transactivation domains in MDM2 recognition.* Cell Cycle, 2015. **14**(4): p. 533-43.
56. Rajagopalan, S., et al., *Mapping the physical and functional interactions between the tumor suppressors p53 and BRCA2.* Proc Natl Acad Sci U S A, 2010. **107**(19): p. 8587-92.
57. Kussie, P.H., et al., *Structure of the MDM2 oncoprotein bound to the p53 tumor suppressor transactivation domain.* Science, 1996. **274**(5289): p. 948-53.
58. Raj, N. and L.D. Attardi, *The Transactivation Domains of the p53 Protein.* Cold Spring Harb Perspect Med, 2017. **7**(1).
59. Bresnick, A.R., D.J. Weber, and D.B. Zimmer, *S100 proteins in cancer.* Nat Rev Cancer, 2015. **15**(2): p. 96-109.
60. Fei, F., et al., *S100A4 in cancer progression and metastasis: A systematic review.* Oncotarget, 2017. **8**(42): p. 73219-73239.
61. Newman, J., *Expanding screening space through the use of alternative reservoirs in vapor-diffusion experiments.* Acta Crystallogr D Biol Crystallogr, 2005. **61**(Pt 4): p. 490-3.
62. Kabsch, W., *Xds.* Acta Crystallogr D Biol Crystallogr, 2010. **66**(Pt 2): p. 125-32.
63. McCoy, A.J., *Solving structures of protein complexes by molecular replacement with Phaser.* Acta Crystallogr D Biol Crystallogr, 2007. **63**(Pt 1): p. 32-41.
64. Gingras, A.R., et al., *Crystal structure of the Ca(2+)-form and Ca(2+)-binding kinetics of metastasis-associated protein, S100A4.* FEBS Lett, 2008. **582**(12): p. 1651-6.
65. Adams, P.D., et al., *PHENIX: a comprehensive Python-based system for macromolecular structure solution.* Acta Crystallogr D Biol Crystallogr, 2010. **66**(Pt 2): p. 213-21.
66. Emsley, P., et al., *Features and development of Coot.* Acta Crystallogr D Biol Crystallogr, 2010. **66**(Pt 4): p. 486-501.
67. Wang, Z.X., *An exact mathematical expression for describing competitive binding of two different ligands to a protein molecule.* FEBS Lett, 1995. **360**(2): p. 111-4.
68. Oh, Y.S., et al., *SMARCA3, a chromatin-remodeling factor, is required for p11-dependent antidepressant action.* Cell, 2013. **152**(4): p. 831-43.

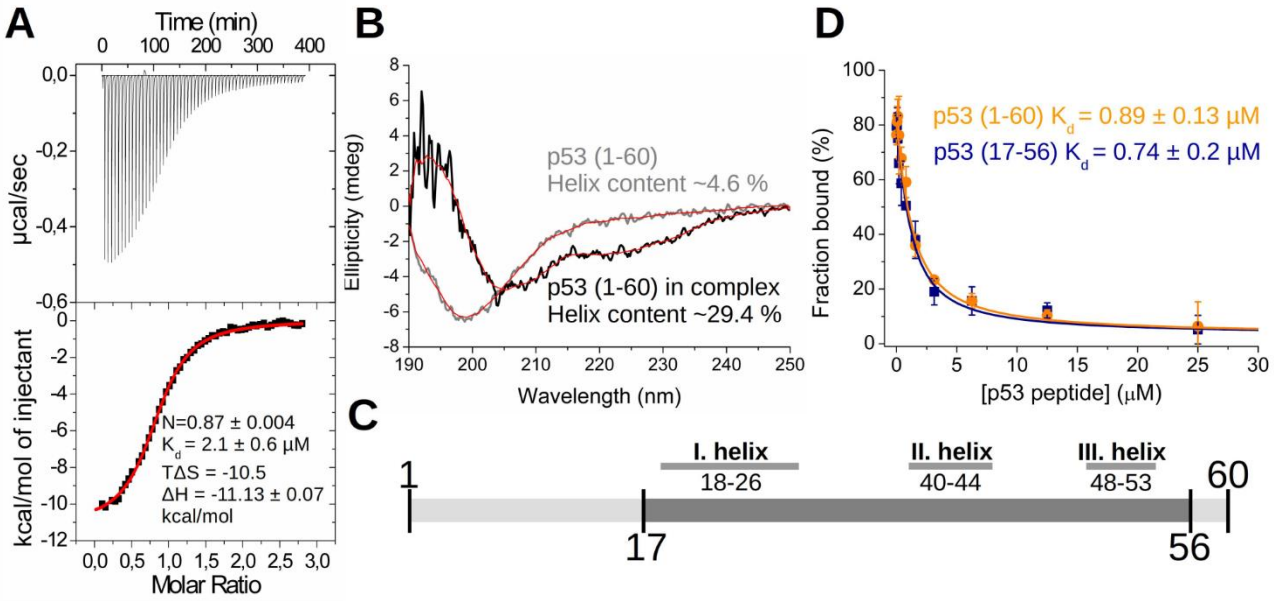

Fig. 1. In vitro characterization of p53 TAD – S100A4 complex (A) 60 µM wild type S100A4 dimer was titrated with 500 µM p53 TAD$^{1-60}$ fragment in an ITC assay. (B) CD measurements show that the intrinsically disordered p53 TAD$^{1-60}$ (light grey) adopts a more α-helical structure upon binding to S100A4 (dark grey). (C) Schematic representation of p53 TAD shows the two fragments that were produced and used in this paper (light and dark grey as p53 TAD$^{1-60}$ and p53 TAD$^{17-56}$ respectively). The three segments with high secondary structure propensity (found by Lee *et. al.* [40]) are highlighted. (D) Fl-p53 TAD$^{17-56}$ complexed with wild type S100A4 were titrated with unlabeled p53 TAD$^{1-60}$ and p53 TAD$^{17-56}$ fragments in an FP assay. Each data point represents the mean ± SD of three independent experiments. Lines represent the fitting of competitive binding equation [67].

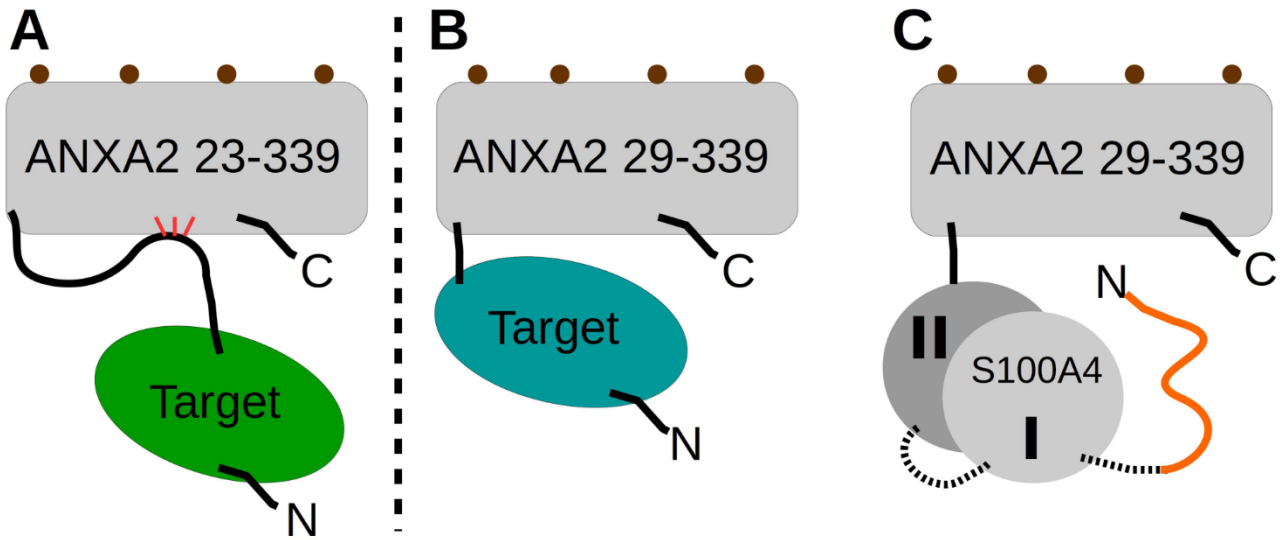

Fig. 2. Schematic representation of the ANXA2 fusion constructs used for the crystallographic studies (A) The target protein is fused to the C-NTD (23-33) of ANXA2. Here the additional interactions between C-NTD and CTD (34-339) (red lines) stabilize the structure of ANXA2. (B) Almost the whole NTD (2-28) is removed and the target protein is fused directly to the first α-helix of ANXA2 core domain (29-339) with a short linker. (C) In the present work the p53 TAD^{17-56} (orange) was fused to the scS100A4Δ8 (I and II represents the subunits), which is fused to $ANXA2^{29-339}$. Dashed lines indicate the GS linkers. Brown dots represent calcium ions.

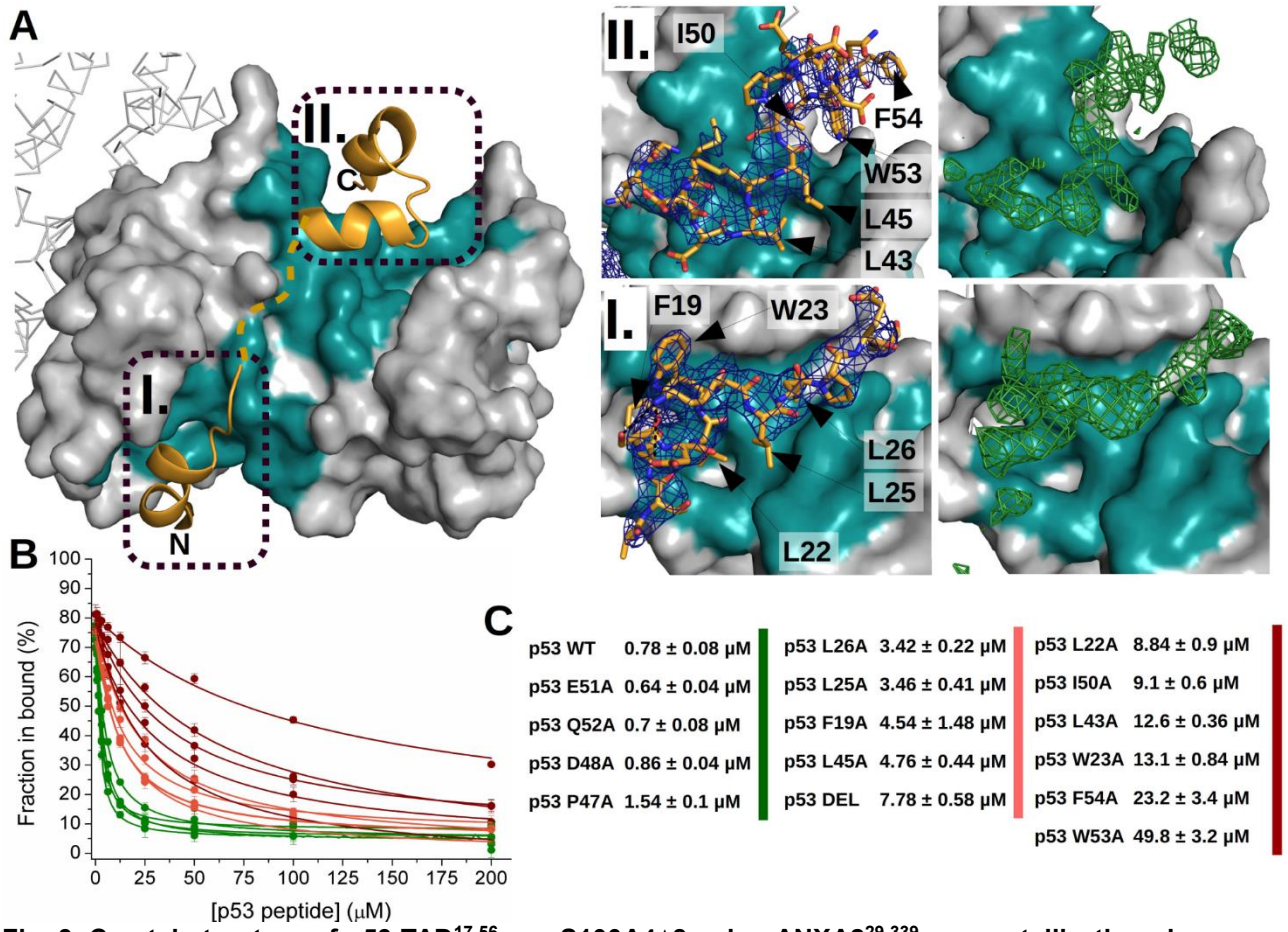

Fig. 3. Crystal structure of p53 TAD$^{17-56}$ – scS100A4Δ8 using ANXA2$^{29-339}$ as crystallization chaperone and its validation using alanine scanning of p53 TAD (A) The binding of p53 TAD$^{17-56}$ (bright orange) to scS100A4Δ8 (grey: S100A4 dimer, teal: the interacting surface). ANXA2$^{29-339}$ is visualized here with grey ribbon. The N- (I.) and C-terminal α-helices (II.) bind to the hydrophobic pockets of S100A4 (formed by the helices 3, 4 and the hinge region of each subunit), while the region in between (dashed line) makes only transient interactions with the first helices of the dimer. The α-helix stabilizing intramolecular interactions of S20 and D21 with K24 of p53 are denoted with black dashed lines. Electron density map of p53 TAD$^{17-56}$ is visualized in blue (final 2Fo-Fc contoured at 1.0 sigma) and the Fo-Fc map of a simulated annealing omit map, generated by omitting p53 peptide, is presented in green (contoured at 2.5 sigma). (B) Fl-p53 TAD$^{17-56}$ complexed with wild type S100A4 were titrated with unlabeled alanine mutants of p53 TAD$^{17-56}$ in an FP assay. Each data point represents the mean ± SD of three independent experiments. Lines represent the fitting of competitive binding equation [67]. (C) The different p53 TAD mutants are grouped by their relative affinity to wild type S100A4. Green column: K_d = 1 – 2 μM; pink column: K_d = 2 – 8 μM; red column: K_d > 8 μM compared to wild-type p53 TAD$^{17-56}$.

Table 1 Data collection and refinement statistics

	p53 TAD$^{17-56}$-scS100A4Δ8-ANXA2$^{29-339}$
Data collection	
Space group	P 1 21 1
Cell dimensions	
a, *b*, *c* (Å)	95.96, 62.77, 106.02
α, *β*, *γ* (°)	90, 90.25, 90
Resolution (Å)*	47.98 -3.1 (3.18-3.1)
R_{meas} (%)*	17.0 (101)
I/σ*	10.0 (1.74)
Completeness (%)*	99.8 (99.9)
Redundancy*	6.68 (5.37)
CC1/2*	99.5 (70.1)
Refinement	
Resolution (Å)	47.98 -3.1
No. reflections*	155290 (9136)
R_{work}/ R_{free}	0.23/0.272
No. residues	
Protein	533
Glycerol	2
Ca^{2+}	8
Water	0
B-factors	
Protein	73.11
Ca^{2+}	77.4
GOL	57.5
Ramachandran	
Favoured (%)	94
Allowed (%)	6
Outliers (%)	0

Data were collected on single crystals
*Highest resolution shell is shown in parenthesis.

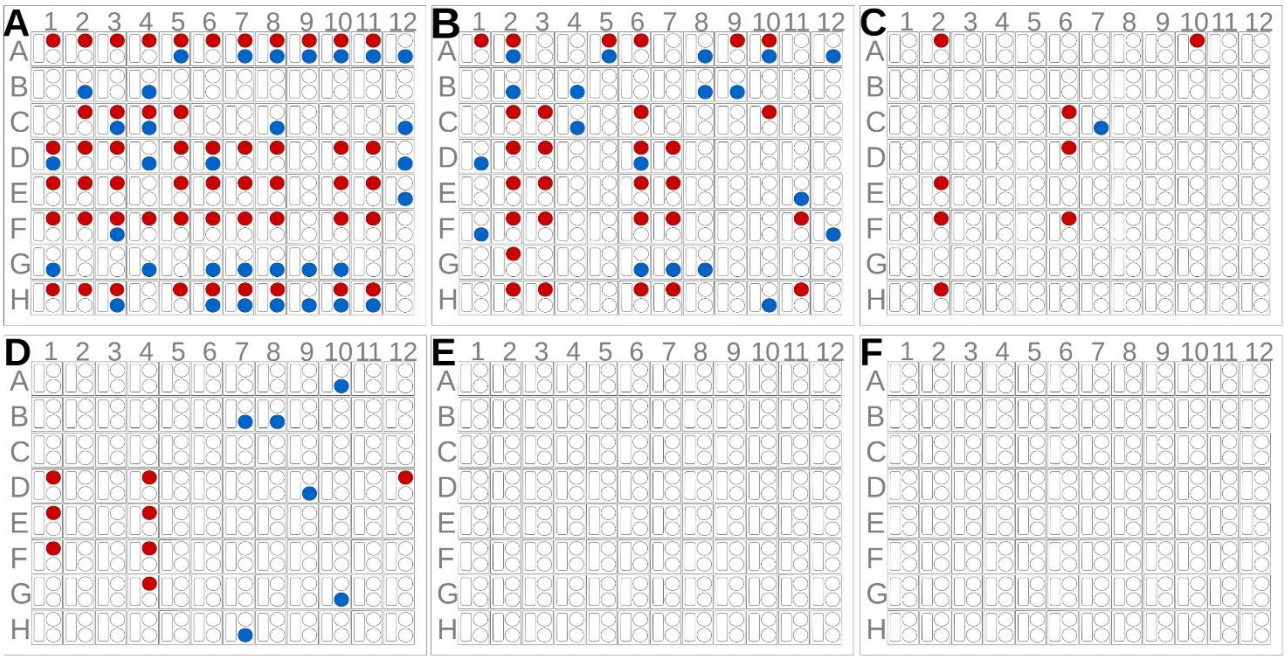

Fig. 4. Crystal screening of different wtMBP and ANXA2 constructs (A) ANXA2$^{29\text{-}339}$ and (B) PDZ-ANXA2$^{23\text{-}339}$ crystals were formed under numerous JCSG+ (blue) and Morpheus (red) crystallization conditions at 250 μM concentration. (C) In case of the larger scS100A4Δ8-ANXA2$^{29\text{-}339}$ construct, crystal formation significantly dropped. Crystal formation of (D) wtMBP (E) wtMBP-PDZ and (F) wtMBP-scS100A4Δ8 at 2 mM concentration. Crystal growth was monitored for a week.

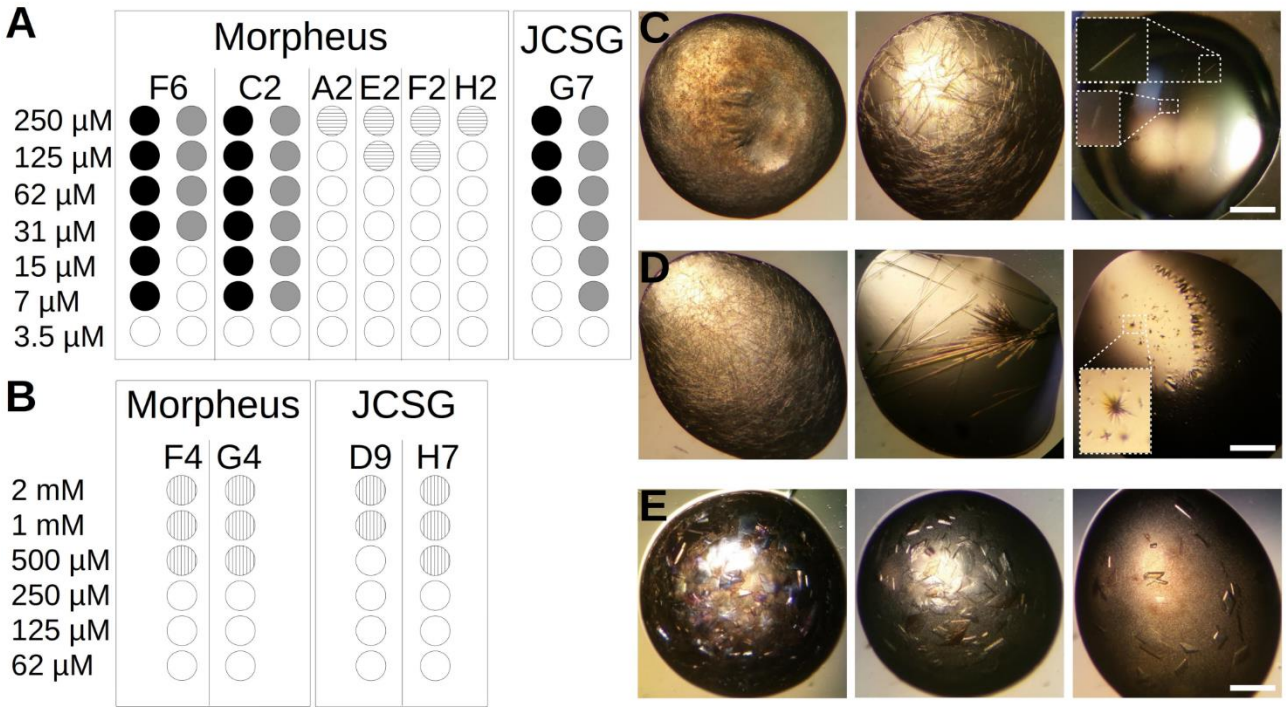

Fig. 5. Crystallization of ANXA2 constructs and wtMBP at different concentrations using the best conditions found in the screening experiments Formation of (A) ANXA2$^{29-339}$ (black), PDZ-ANXA2$^{23-339}$ (grey) and scS100A4Δ8-ANXA2$^{29-339}$ (horizontal lines) crystals were monitored at different protein concentrations for a month. (B) MBP crystals (vertical lines) formed only at higher than 500 µM concentration (~20.5 mg/ml). No MBP fused constructs were tested since no hit was found during screening. (C) PDZ-ANXA2$^{23-339}$, (D) ANXA2$^{29-339}$ (E) wt MBP crystals when samples were used at 250 µM (2mM), 62.5 µM (1mM) and 7 µM concentrations (0.5mM) from left to right (wtMBP concentrations are in parenthesis). Small crystals are highlighted in white boxes. White bars represent 0.5 mm.

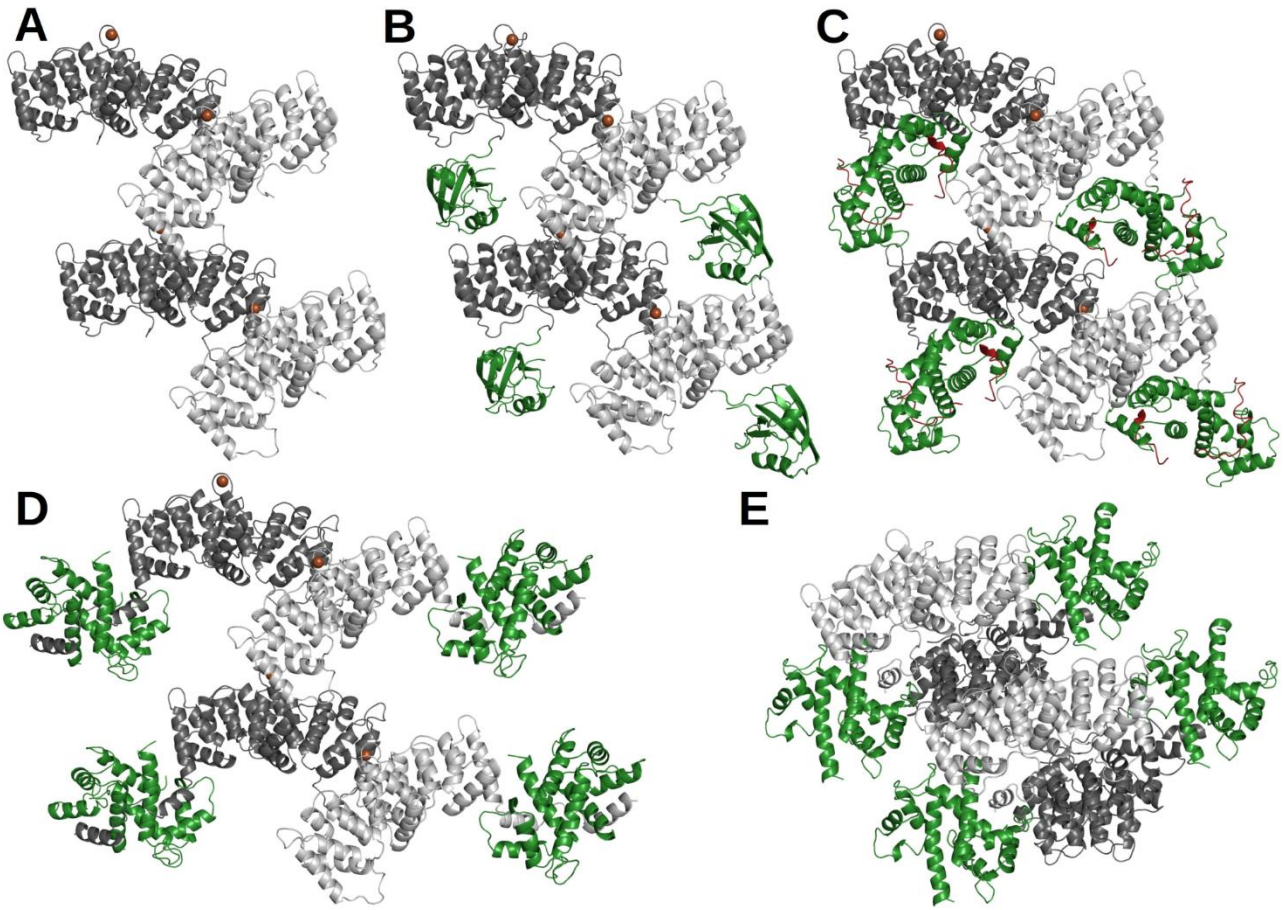

Fig. 6. Crystal packing of ANXA2 in structures found in the PDB (A) ANXA2 in Ca^{2+}-bound form (PDB: 1XJL, light and dark gray) produces elongated crystal lattices (same in 5LPX, 5LQ0, 2HYW, 4X9P and 5LQ2 structures). Structures of previously solved (B) PDZ-ANXA2$^{23-339}$ (PDB: 5N7D, PDZ in green), (C) p53 TAD$^{17-56}$–scS100A4Δ8-ANXA2$^{29-339}$ (PDB: 6T58; p53 TAD$^{17-56}$ in red and scS100A4Δ8 in green) chimeras and the (D) S100A4 – ANXA2 complex (PDB: 5LPU, S100A4 in green) keeps this crystal packing mode. (D) In case of the native, non-fused S100A4 – ANXA2 complex, the S100A4 dimer leaves the ANXA2 formed pockets and localizes beside the molecules. (E) S100A10 binds ANXA2 in a Ca^{2+}-independent manner (PDB: 4HRE) [68]. Here the observed crystal contacts does not form. S100A10 binds two ANXA2 proteins allowing the formation of a different crystal packing mode.

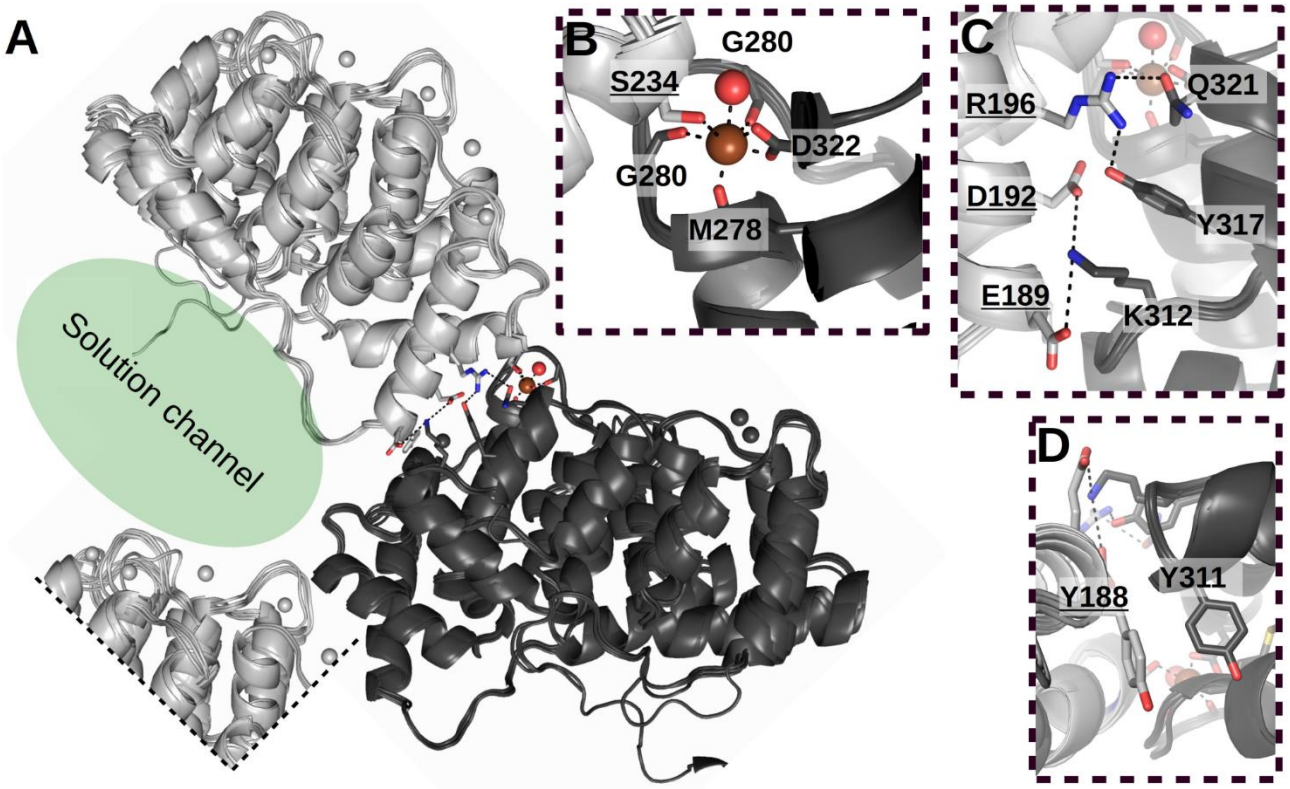

Fig. 7. Crystal contacts of two ANXA2 molecules (A) The aligned ANXA2 structures (PDB: 5LPX, 5LQ0, 5LPU, 1XJL, 2HYW, 4X9P and 5LQ2) shows the conservative crystal contacts. The additional segments of the crystal lattice (light gray ANXA2s are in identical position) defines the solution channel (green ellipse) formed in ANXA2 crystals. (B) S234 of light gray (molecule B) ANXA2 helps the coordination of Ca^{2+} (brown sphere) connecting to dark grey ANXA2 (molecule A). (C) Besides Ca^{2+} coordination, residues of the nearby α-helices form ionic, while (D) two tyrosines form hydrophobic interactions, further stabilizing the assembly. Residues of molecule B are underlined.